

## Unified Hybrid Inception Using Hybrid Neural Encoder-Decoder for AMD Detection on Retinal Fundus Images

A. Bali\*, K. Singh, V. Mansotra

Department of Computer Science and IT, University of Jammu, Jammu-180016, J&K, India

Received 27 December 2023, accepted in final revised form 14 May 2024

### Abstract

Age-related macular degeneration (AMD), a common eye illness that can cause significant vision loss in older persons, can also result in visual loss. It is a medical issue that is primarily brought on by aging. In this paper, a combinative method is presented using U-Net with a modified Inception architecture for the diagnosis of AMD disease. The proposed method is based on deep neural architecture formalizing encoder decoder modeling with convolutional architectures, namely Inception and Residual Connection. The performance of the proposed model was validated on the ADAM AMD Dataset. Experiments demonstrate that the modified Inception deep feature extractor improves AMD classification with a classification accuracy of 92.5 % and segmentation accuracy of 99 % in ADAM across classes in comparison to Resnet. The paper tests the dataset with the proposed model of Hybrid Dense-ED-UHI: Encoder-Decoder based U-Net Hybrid Inception model with 15-fold cross-validation. The paper, in detail, discusses the various metrics of the proposed model with various visualizations and multifold validations.

*Keywords:* Age-Related Macular Degeneration (AMD); ADAM; InceptionV3; UNet; ResNet18; ResNet34; Segmentation.

© 2024 JSR Publications. ISSN: 2070-0237 (Print); 2070-0245 (Online). All rights reserved.  
doi: <https://dx.doi.org/10.3329/jsr.v16i3.70620> J. Sci. Res. **16** (3), 663-679 (2024)

### 1. Introduction

The quality of one's vision is a key sign of one's health and well-being. According to estimates, approximately 3.3 million elderly Americans have visual problems, and the population of adult Americans by means of loss of visualization is expected to increase. The number of individuals affected by blindness is projected to double from 1.02 million in 2015 to 2.1 million by the year 2050. Currently, over 12 million people aged 40 and above are experiencing some form of vision impairment. Recently, substantial advancement has been achieved in terms of improving drug delivery to internal eye tissues and maintaining effective therapeutic dosages within some of these body tissues. The majority of pharmacologic ocular disease care continues to rely on the topical delivery of solutions to the eye's surface as drops. Dry eye is a visual disorder that causes distress, visual disruption, and tear film instability. In addition, it is the risk for eye disorders and supplemented by an

---

\* Corresponding author: [akankshabali5@gmail.com](mailto:akankshabali5@gmail.com)

increase in the osmolarity of the tear film as ocular surface irritation. Neovascularization of the eye is linked to a variety of diseases, typically resultant in considerable vision loss and eventually blindness. The most frequently affected patients in the Western world seem to be age-related macular degeneration (AMD) and diabetic retinopathy (DR). It is necessary to describe the varied procedures connected with the pathogenesis of AMD and DR to evolve medications and eventually eliminate loss of vision and blindness. According to the reinforcement analyses of different population-based research conducted in industrialized and developing economies, age-related eye disorders such as macular degeneration, glaucoma, diabetic retinopathy, and cataracts are the primary causes of vision loss. Vascular endothelial growth factor-A (VEGF-A) is a protein that is involved in the incidence and progression of DR and AMD [1,2].

Treatment for age-related eye illnesses is expensive, and it impedes older people's ability to live independently. It also increases the risk of accidents and deaths. A high dosage of antioxidants (vitamin E, vitamin C, and beta carotene) and zinc as zinc oxide was given to patients who are suffering from AMD or advanced AMD. On the basis of these determinations, the AREDS Research Group and others suggest that communities with these characteristics who do not have any contraindications recognize health supplements.

Blindness and vision loss can result from diseases of the fundus. A few frequent fundus conditions that impair vision are cataracts, diabetes retinopathy, and age-related macular degeneration. The first illness of the eyes that causes total blindness is AMD [3]. AMD impairs central vision, whereas distortion and blurring impact peripheral vision. There are two types of AMD: wet AMD (exudative AMD) and dry AMD (non-exudative AMD). If dry AMD is present, the retinal pigment epithelium behind the retina deteriorates. Loss of the central photoreceptors in the retina causes visual loss. The primary symptom and initial clinical sign of dry AMD are drusen or subretinal deposits generated by retinal waste products. Wet AMD results in vision loss as a result of the choriocapillaris' aberrant blood vessel proliferation, which eventually leads to blood and protein leaks beneath the macula. If left untreated, the bleeding, scarring, and leakage from these blood vessels eventually kill the photoreceptors irreversibly and result in unexpected vision loss. The main indication of wet AMD is exudation [4].

The world of today requires automated and precise diagnostic procedures. The automation of the detection/prediction procedure for various eye illnesses has advanced significantly with the introduction of Deep Learning (DL) and image processing techniques. The use of technology for early disease diagnosis has become more prevalent and has made it easier to get information. Computer vision deep learning models have rapidly advanced. Image features can be automatically learned by convolutional neural networks. In terms of target detection and image categorization, they did well. Their capacity for representation makes up for the shortcomings of conventional picture extraction. The innovative technique has also been used in the medical field to enhance the management of a number of health issues. The conditions that received the most research attention were glaucoma, AMD, and diabetic retinopathy [5].

Due to the many morphologies, sizes, and colors of lesions, manual retinal lesion assessment is laborious and demands great accuracy. Computer-assisted diagnostic (CAD) tools make it possible to diagnose AMD accurately and quickly, which helps with choosing the best course of action. To examine the Region of Interest (ROI) and determine the grade and severity of the disease, AMD lesion segmentation is essential. Because Machine Learning (ML) techniques are more precise than traditional segmentation methods that rely on few indicators, they have taken their position. The integration of machine learning and artificial intelligence (AI) has demonstrated significant promise in the identification and diagnosis of AMD in recent years. Large datasets of retinal pictures can be analyzed using this technology to find subtle patterns and biomarkers linked to AMD. The benefit of adopting machine learning algorithms is that they can learn and develop over time, resulting in more precise and effective AMD detection. The figure below shows normal vision, Dry AMD, which is identified by the formation of yellow deposits in the macula known as drusen that eventually erode and thin the macular tissue. The final image shows wet AMD, which is less prevalent but more severe and can result in a quick and severe loss of eyesight. It happens when unnatural blood vessels develop behind the retina and begin to leak fluid or blood, causing macula damage. The central vision may suddenly become distorted or have blind areas due to wet AMD [6]. Fig. 1 displays fundus photos of normal, Dry AMD, and Wet AMD images.

In comparison to conventional ML algorithms, DL, a contemporary technology, has demonstrated improved performance in AMD lesion classification and segmentation.

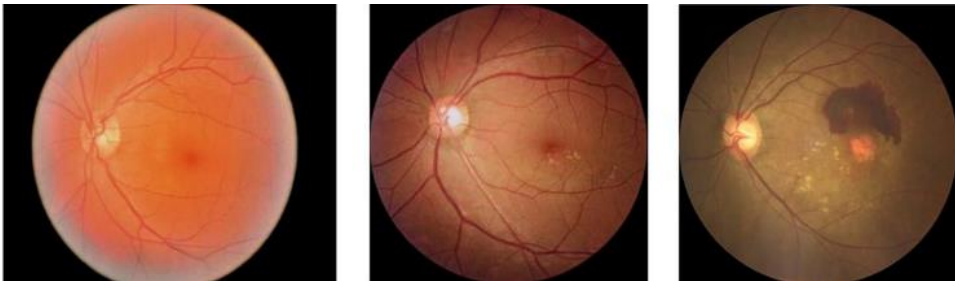


Fig. 1. a) Normal, b) dry AMD, abd c) wet AMD [7].

In recent years, deep neural networks and particular machine learning models have shown promise in a variety of computer vision applications, particularly in the area of medical picture analysis for AMD. Deep learning-based computer-aided diagnostic (CAD) systems that can categories anomalies can aid in medical decision-making and enhance patient care [8]. The rest of the paper is structured as follows. Related works on AMD image classification are presented in Section II. The information and suggested approach are explained in Section III. The experimental analysis and discussion are presented in Section IV. Section V presents the conclusions at the end.

## 2. Literature Review

Hong *et al.* [9] developed a 14-layer deep CNN model that may help ophthalmologists with ocular screening and diagnose conditions in the early stages of AMD. Ten fundus illnesses were classified using neural networks and random forests in the structured analysis of the REtina (STARE) database [9].

The random forest classifier and VGGNet feature are both inadequate for visual identification, even with the rapid progress in deep learning. Numerous programs have been classified as multi-modal AMD [10]. Using color fundus and OCT scans, Yoo *et al.* [11] classified patients into three classes: normal, dry AMD, and wet AMD. Similar to the single-modal scenario, the authors extract visual characteristics from both modalities using a pre-trained VGG19 model. After that, the characteristics are combined and sent as input to a random forest classifier. Because there are fewer paired multi-modal training examples than single-modal training instances, training a multi-modal network is challenging. Consequently, a multi-modal CNN will perform better than its single-modal competitor. Visual interpretation of the contribution of each modality to the final categorization is not possible using this approach. Clinical decision support (CDS) systems have seen a surge in diagnostic use during the last ten years.

Author Govindaiah *et al.* [12] looked at the effectiveness of DCNN screening for age-related macular degeneration (AMD). An enhanced VGG16 neural network with batch normalization is being studied and analyzed, and the training dataset is the more than 150,000-image Age-Related Eye Disease Study (AREDS) dataset. The investigation's findings showed that completely training a deep neural network outperforms utilizing pre-trained network categorization when there is sufficient training data, especially in AMD diagnosis and screening.

A lot of studies have also been done on AMD categorization. Transfer learning using ImageNet pre-trained models, namely the Inception network, was shown to be very effective in the categorization of eye diseases. Using several base networks for ensemble learning might further enhance classification performance. These experiments show that using CNNs to achieve great sensitivity is feasible [13]. Additionally, DCNN has been shown to outperform conventional image analysis methods in a number of areas, most notably feature extraction. Recently, color fundus pictures were detected using DL approaches, and the results were promising even though the greatest occurrences of responsiveness and accuracy were, in reality, lower than those achieved using state-of-the-art methods. Ganjdanesh *et al.* [14] presented a novel deep learning-based classification model (LONGL-Net) on 30,000 images of the custom dataset that has the ability to predict the longitudinal result or whether the patient would be in late-AMD at a future time-point and grade the current fundus images at the same time. AUC (Area Under Curve) of 90.5 % and accuracy of 76.2 % had been achieved by the author on the three-class classification. Using a deep learning (DL) scheme with serially concatenated deep and handcrafted features, Kadry *et al.* [15] developed an automated system for detecting age-related macular degeneration (AMD) and achieved an accuracy of 97.08 %. For multiclass multilabel

classification on the ODIR-19 dataset, Bali *et al.* [16] proposed a one versus-rest classifier and achieved 90.45 % validation accuracy and 98.29 % training accuracy on AMD diagnosis. Bali *et al.* [17] proposed a DFex-hybrid approach of the BeeHive model, CGAN, and PSO to categorize eye diseases and obtained 98.79 % accuracy, 95.99 % sensitivity, 99.79 % specificity and 97.16 % accuracy, 96.81 % F1 score in the RFMiD and ODIR dataset respectively. Ogundokun *et al.* [18] proposed a novel deep transfer learning approach for AMD detection and achieved an accuracy of 96.41 %, precision of 94.24 %, specificity of 94.82 %, false positive rate (FPR) of 0.0518, and area under receiver operator characteristics curve of 0.9633 on the test set. Ajesh *et al.* [19] applied PSO and deep neural techniques on the AREDS dataset and attained a sensitivity of 0.97, specificity of 0.97, accuracy of 0.96, and detection rate of 0.94.

Table 1 presents the various methods derived from AMD fundus photos and tabular data of the most recent literature study on the ADAM dataset.

Table 1. Tabular representation of the state-of-the-art literature review on the ADAM dataset.

Author	Objective	Tech. used	Result	Remark
Morano <i>et al.</i> [20]	To provide a deep learning method that can be explained for diagnosing AMD by jointly identifying the retinal lesions that are connected with it.	Custom CNN	AUROC: 93.62 %	<ul style="list-style-type: none"> <li>• Computationally intensive.</li> <li>• Appropriate for individual pathology investigations</li> </ul>
Niu <i>et al.</i> [21]	To decrease the number of false positives in the normal structure by proposing the Region and Spatial Aware Anomaly Detection (ReSAD) approach for fundus imaging, which gathers local region and long-range spatial information.	Transfer Learning	Accuracy: 73.2 % AUC: 82.0 %	<ul style="list-style-type: none"> <li>• Accuracy and AUC can be improved.</li> <li>• Parameter tuning may be required.</li> </ul>
Tang <i>et al.</i> [22]	To present a U-Net backbone enhanced with hierarchical bottleneck detection for Degenerative Retinal Fundus Images Landmark Detection	HBA-U-Net	Euclidean Distance: 25.4 pixels; Dice Coefficient: 94.7 %	<ul style="list-style-type: none"> <li>• Automated Feature Learning</li> </ul>
Proposed	To develop an automated AMD diagnostic approach.	Hybrid Dense-ED-UHI	Classification Results: Test AMD Accuracy: 92.5 %; Non-AMD Accuracy: 92.5 %; Segmentation Results: Accuracy: 99.4 %, AUC: 99.1 %.	<ul style="list-style-type: none"> <li>• High Accuracy and AUC.</li> <li>• Automated feature learning.</li> <li>• Can handle small or imbalanced datasets</li> </ul>

The goal of this paper is to develop an automatic diagnosis method for AMD. The paper discusses multiple deep-learning techniques for the segmentation of the fundus image. The paper is capable of not only reducing the computation time for the enhanced Dense-ED-UHI: Encoder Decoder-based Unet Hybrid Inception architectures but also is able to hybridize it with inception V3 to calculate complex features for better extractions.

Considering the aforementioned review, we developed a unique architecture to overcome the aforementioned restrictions. The following is a description of the main contributions of the suggested research efforts:

- 1) This work segments retinal lesions semantically using a customized U-Net model. "InceptionV3" is the name of the deep network encoder that was utilized in the model. Training may be completed more quickly using the InceptionV3 model because of its smaller convolutions.
- 2) The model uses a special up-sampling method that includes pixel-wise periodic shuffling convolution to enlarge the convolution closest neighbor. Our method produces retinal pictures with outstanding resolution and no checkerboard artifacts, and it does so faster than conventional methods.
- 3) The proposed approach yielded state-of-the-art results for AMD diagnosis when compared to previously published publications.
- 4) The work uses a hybrid U-Net architecture with numerous kernel extractions and an inception design to infect deep encoding.
- 5) Lastly, the research assesses how well the model performs in various classes.

### **3.1. Data and methodology**

The methodology, experiment design, and workflow employed in the proposed framework were used in this section's full explanation of the dataset.

### **3.2. Dataset**

The Zhongshan Ophthalmic Center at Sun Yat-sen University in China supplied 1200 retinal fundus photos that are recorded in JPEG format with 8 bits per color channel, which make up the ADAM dataset. A Zeiss Visucam 500 fundus camera with a resolution of 2124 x 2056 pixels (824 photos) and a Canon CR-2 device with a resolution of 1444 x 1444 pixels (376 photographs) were used to capture the fundus images [23].

### **3.3. Implementation details**

A GPU equipped with 8 GB of RAM was employed for training models. In a study [24], image segmentation using U-Net was explored, marking one of the initial investigations into this approach. The work specifically focused on utilizing the U-Net architecture for segmenting retinal lesions in AMD images. Since then, the application of U-Net has expanded beyond AMD detection, becoming widely adopted across various medical image segmentation tasks. Originally designed for general biomedical image segmentation, the U-

Net architecture is now extensively utilized in diverse medical imaging domains, including AMD. The model employed in this study underwent 200 epochs with a learning rate of 0.001, a batch size of 16, consisting of 6 encoders and 6 decoders, incorporating L1 regularization, utilizing Sigmoid activation across the network, Relu activation in the predictive space, Adam optimizer, and employing a loss function composed of 90 % Dice Loss and 10 % Focal Loss.

Although the U-Net design has shown beneficial in segmenting retinal structures and lesions in pictures of AMD, it is not without limitations. There are several limitations when using U-Net for AMD, such as its limited ability to gather global context. Because U-Net relies heavily on local information due to its encoder-decoder design, it may not be able to consider larger spatial linkages and contextual signals. This limitation could make it more difficult for the model to include global variables that are required for accurate classification of AMD, which might be detrimental to the model's overall effectiveness. To overcome this constraint, more architectural modifications or the addition of other approaches may be needed to enhance the integration of global context and raise the classification accuracy.

Rather than using the traditional U-Net architecture, the research incorporates ideas from the Inception design into a neural network. When many kernel sizes are used in the Inception design to gather data at different granularities and on different scales, the detection process becomes easier. Furthermore, U-Net Inception enhanced feature representation, which resulted in a deeper understanding of the retinal picture and could enhance the overall performance of the proposed model. Furthermore, the incredibly accurate segmented output picture is produced with the aid of expansive to-contract cross-linking. The U-Net contract chain consists of four encoder unit blocks. A max-pooling layer comes after the two convolution layers in each encoder unit. Features are multiplied each time a pooling method is used. The key element between contractile and expanded approaches is the bottleneck, which is made up of two convolution layers, one at the top. Four decoder units are doing a U-Net expanding route, which comprises two convolution layers, one de-convolution layer, and two similar feature maps that make use of the contract trail.

The process that is shown in Fig. 2 is composed of the workflow stages. The dataset's training, testing, and validation sets are divided into the following ratios: 70:20:10. All of the images have been resized to 512\*512 after the data has been preprocessed. The next step was data normalization, which gave each variable an equal weight to prevent any one variable from adversely affecting model performance just because it contained large numbers. This increased model accuracy. We converted the category data into numerical data by performing a single hot encoding after normalization since our technique is limited to processing numeric data. This makes it possible for us to use our strategy without running into any problems.

A single algorithm cannot be utilized to segment all the photographs since the area of interest varies based on the application. As a result, many hybrid segmentation strategies are used, such as unet res18, unet res34, unet inception, and so on. A fresh layout dubbed "inception-Unet" is a hybrid of the inception and unet architectures, two state-of-the-art

deep learning algorithm designs. The default convolution layers in the unet are replaced with the inception layers. Unet's primary function is to process biological images, which have developed from conventional CNN. CNN specializes in image classification problems, where the input is an image and the output is a label. Unet is used to categorize each pixel in the picture since, under biological situations, we must not only determine if disease exists but also pinpoint the region of abnormalities.

The large fluctuation in the location of the information makes choosing the right kernel size for the convolution process challenging. The inception module utilizes a range of filter sizes as a consequence, with bigger filters covering more information and smaller filters covering less. After that, the validation dataset is used to evaluate and confirm the model. For instance, overfitting occurs if the training accuracy is 10 % greater than the validation accuracy, while underfitting occurs if the training accuracy is 10 % lower than the validation accuracy. Both occurrences have included hyperparameter tuning, which involves automatically adjusting various parameters. The iterative mode is continued, the model is stored, and 10-fold cross-validation is carried out on an 80:20 ratio until there is no longer any overfitting or underfitting.

A deep learning method called cross-validation assesses the model's performance on unseen data. One-fold or subset of the data is the testing set, while the other data is the training set. The last step involves averaging the outcomes from each testing phase to get a more reliable evaluation of the model's output. Preventing overfitting, which occurs when a model performs badly on unknown data while having been trained exceedingly well on training data, is the main objective of cross-validation. Other performance indicators, such as the sensitivity, recall, and f1 score, were then calculated.

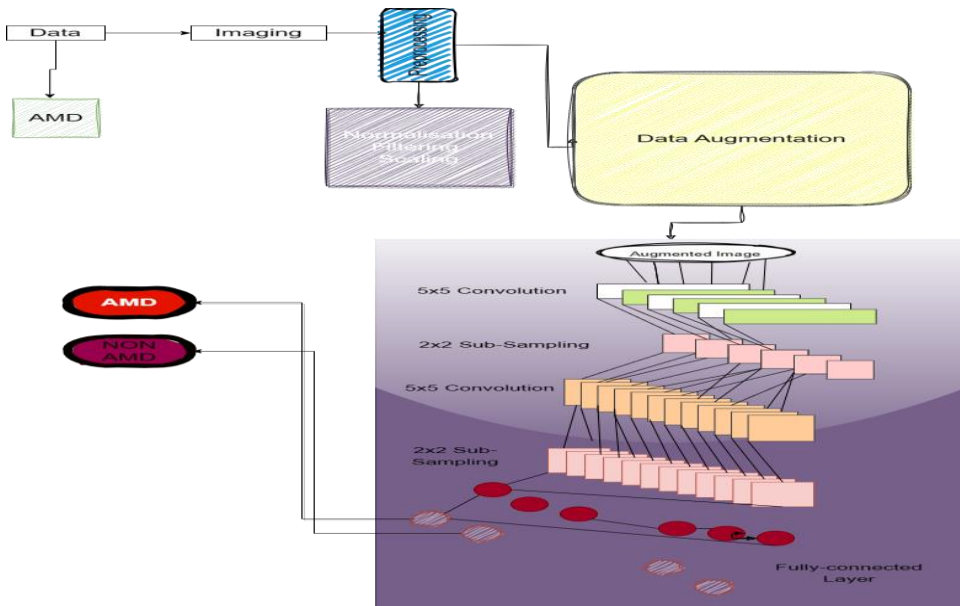


Fig. 2. Suggested workflow.



Fig. 3 below provides a detailed discussion of the proposed work using the dataset divided into the training, validation, and testing set for AMD classification in retinal photographs.

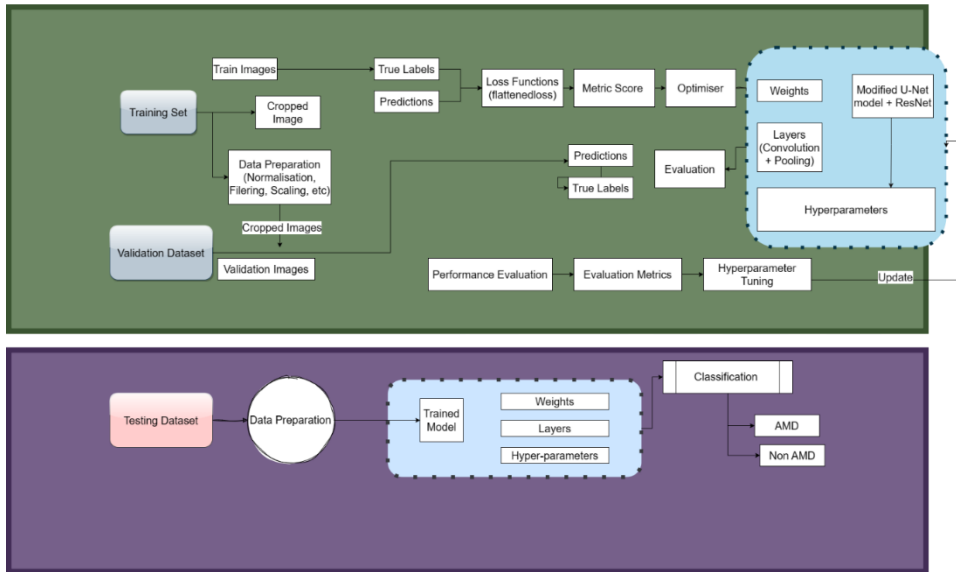


Fig. 3. Detailed overflow of data split.

The research presents a comprehensive workflow that uses the ADAM dataset to train the pictures, adhere to the procedures, and update as needed, as shown in the above figure. After that, the dataset is tested, and if the model meets the predetermined performance standards, it may be used to the medical imaging industry. The suggested U-Net Inception model for AMD classification is discussed in the above graphic. The main goal of the figure is to show how training and testing sets are routed through different preprocessing pipelines, and then the train images are separated using the deep network's loss function and back propagation utilities, which include layers, weights, biases, and hyperparameters.

Figs. 2 and 3 outline the first stages in data preparation in the following sequence.

1. Training: As previously said, 70 % of the training data is utilized to train and repeat the model. Testing and Validation Are Separated. The method of testing and validation is used to analyze the fitting parameter and guarantee accurate modeling.
2. Data preparation, which includes a number of procedures, including scaling, filtering, and normalization of the input sequences.
3. To build a binary mask for many classes utilized, mask encoding, also known as one hot encoding, is performed.
4. The discussion of model development, hyperparameters, and other units follows.
5. After the training cycle is over, the model undergoes a thorough assessment for cross-validation using all relevant measures, including sensitivity, specificity, accuracy, and precision.

## 4. Results and Discussion

### 4.1. Classification

A prevalent eye condition known as AMD (Age-related Macular Degeneration) damages the macula; this is a region of the retinal in the center that is important for crisp and comprehensive perception. For swift action and successful therapy, early AMD screening and categorization are essential. In order to accurately and effectively classify AMD, Deep convex neural networks (DCNNs) have become effective methods for automated retina image processing.

DCNN-based AMD ocular categorization is necessary for a number of reasons. First of all, AMD is a major factor in blurred vision in older people, and prompt diagnosis can lessen the severity of visual impairment. Traditional techniques of AMD categorization rely on ophthalmologists performing manual examinations, which are laborious, personal, and susceptible to inaccuracy. Deep neural networks offer an automatic and impartial method, lessening the workload.

There are numerous advantages to employing DCNNs for AMD retinal categorization. First, DCNNs can quickly analyze enormous volumes of retinal pictures, enabling the evaluation of many individuals in a short amount of time. This flexibility is particularly useful for screening programs that target at-risk populations or regions with poor supply of eye doctors. The precision and sensitivity of AMD diagnosis are further improved by DCNNs' ability to identify minute trends and traits in macular pictures that aren't always readily visible to the naked eye.

Deep neural networks have a chance to continuously track the development of AMD. Frequent visual imaging allows for the early detection of medical abnormalities and swift treatment. The capacity to monitor illness development over time improves the effectiveness of therapy and can aid in the improvement of individuals' personalized treatment programs. Fig. 4 represents the loss and accuracy plot for AMD classification.

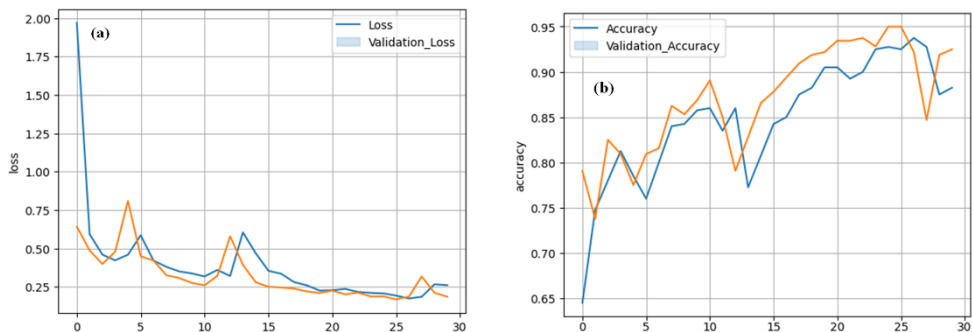


Fig. 4. Loss and accuracy plot for AMD classification.

Table 2. Class wise metric distribution.

Split	class	Accuracy	Precision	Recall or Sensitivity	F1 Score	Specificity
Train	AMD	0.925	0.925373	0.984127	0.953846	0.705882
	Non-AMD	0.925	0.923077	0.945882	0.9180047	0.984127
TEST	AMD	0.925	0.917910	0.991935	0.953488	0.944444
	Non-AMD	0.925	0.961538	0.9294444	0.916452	0.991935

Table 2 offered measurements, including accuracy, precision, recall (or sensitivities), F1 score, and specificity, which may be used to assess the algorithm's effectiveness. These indicators reveal how effectively the algorithm categorizes AMD and non-AMD situations.

The algorithm obtains a 92.5 % accuracy in its initial training set. This indicates that the algorithm properly classifies 92.5 % of the instances in the initial data set. The AMD category has an accuracy of 92.54 %, meaning when the algorithm correctly identifies an instance as having AMD, it does so 92.54 % all the time. The simulation successfully detects 98.41 % of the real AMD cases according to its recall (or sensitivities) for the AMD class, resulting in 98.41 %.

In general, the algorithm performs well in categorizing AMD and non-AMD instances. Excellent precision means a high proportion of correctly classified data was obtained. The algorithm appears to be successful in recognizing true AMD instances based on its elevated recall/sensitivity ratios for the AMD category. The algorithm can correctly identify non-AMD cases according to the high level of specificity scores associated with the non-AMD category. The F1 score, which considers both recall and accuracy, shows that the two criteria are well-balanced.

**Loss:** The amount of this parameter represents how successfully the algorithm is reducing its forecasting mistakes throughout training. In general, it is preferable to have a lower loss amount because it indicates that the algorithm is successfully gaining knowledge on its training information and advancing towards accurate forecasts. In this instance, the resulting loss figures for each of the train (0.002469), testing (0.007438), and validate (0.003827) datasets are all reasonably low, demonstrating the model's efficacy in reducing errors.

**Accuracy** generally quantifies how accurately the projections of the model were made. It shows what portion of the total samples were successfully categorized. The model appears to perform extraordinarily well, obtaining excellent precision across every set of data (train: 99.9979 %, test: 99.9801 %, validation: 99.9933 %), as indicated by the precision numbers in the table. **AUC (Area Under the Curve):** For jobs requiring data with imbalances, AUC is a frequently used statistic to assess algorithms for classification. It assesses how well the model can distinguish between positive and negative samples. A greater AUC score indicates improved efficiency. The areas under the curve (AUC) in the following table (train: 99.9947 %, test: 99.9123 %, validation: 99.9848 %) show outstanding prejudiced ability for all data.

The degree of specificity, sometimes referred to as the genuine negative percentage, gauges how well the algorithm can recognize the negative category. It measures the

accuracy of the model in properly recognizing backgrounds or unsegmented areas in the setting of segmenting medical images. The approach appears to be successful in properly recognizing the non-segmented areas based on its high sensitivity ratings across all data (train: 99.9993 %, test: 99.997 %, validation: 99.9973 %). Fig. 5 represents class-wise prediction results for the AMD and Non-AMD classes.

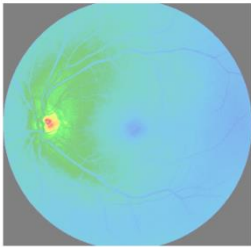
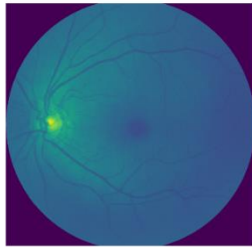
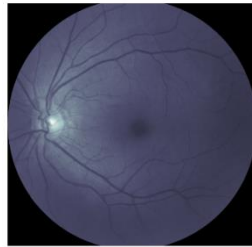
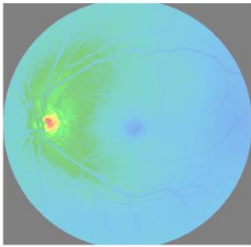
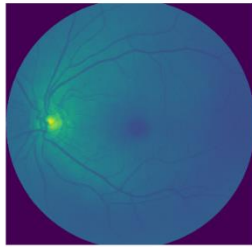
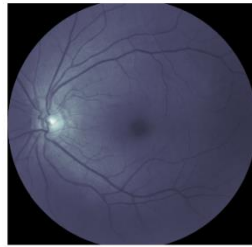
Class	Sample Result		
AMD			
Non-AMD			

Fig. 5. Class wise prediction.

#### 4.2. Segmentation

The method yields comparatively low loss rates for any given collection of data. The system effectively reduces its prediction errors during training, as shown by its average train loss of 0.002469. Table 3 displays the loss, accuracy, binary accuracy, area under the curve (AUC), specificity, and sensitivity values for the training, testing, and validation datasets. The results indicate consistently high performance across all metrics, with negligible differences between the datasets. Though they are somewhat larger, the test and validation losses in Table 3 (0.007438 and 0.003827, respectively) seem to indicate that the algorithm does a respectable job of reducing the differences between the predicted and actual ophthalmic divisions.

The accuracy scores for the test and train sets are also rather high, at 0.999801 and 0.999979, respectively, as Fig. 6 illustrates. This suggests that the algorithm classifies pixels as AMD or non-AMD areas with a high level of overall accuracy. With test and train values of 0.999979 and 0.999801, respectively, the binary accuracy scores further demonstrate the model's ability to categorize pixels reliably. The predictions for inception overlap and mask are shown in Figs. 6 and 7, along with a comparison to Resnet.

Table 3. Performance metrics summary.

SPLIT	loss	accuracy	binary accuracy	auc	Specificity	Sensitivity
Train	0.002469	0.999979	0.999979	0.999947	0.999993	0.998745
Test	0.007438	0.999801	0.999801	0.999123	0.99997	0.988113
Valid	0.003827	0.999933	0.999933	0.999848	0.999973	0.996722

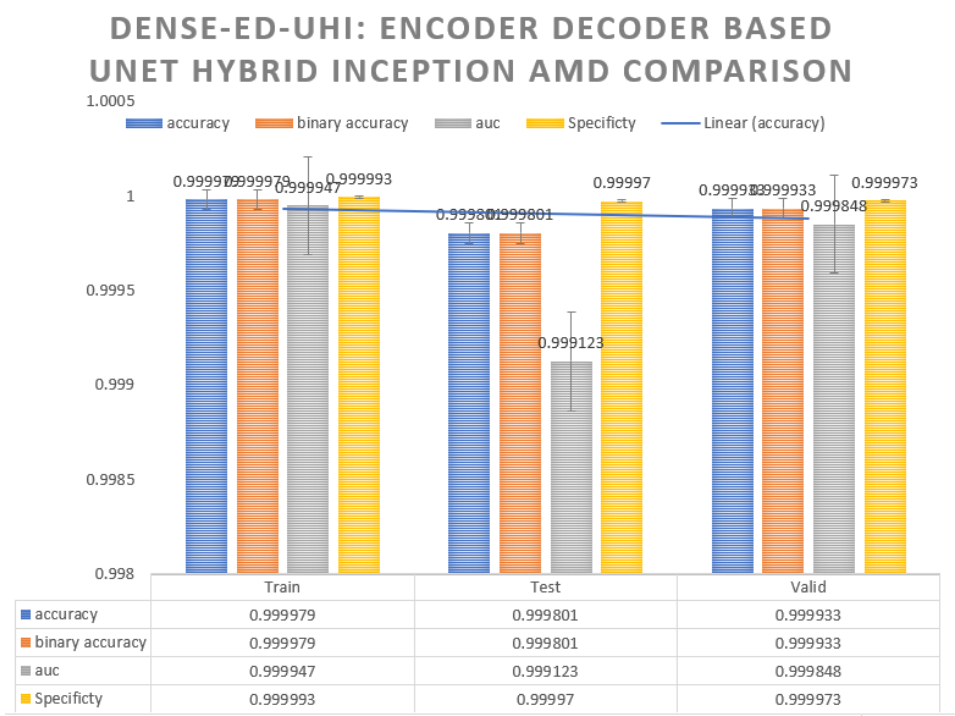
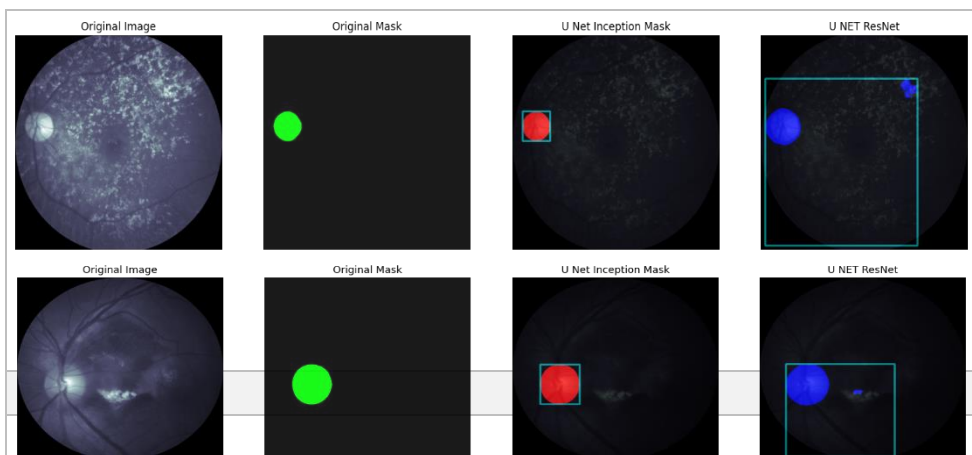


Fig. 6. UHI metric analysis.



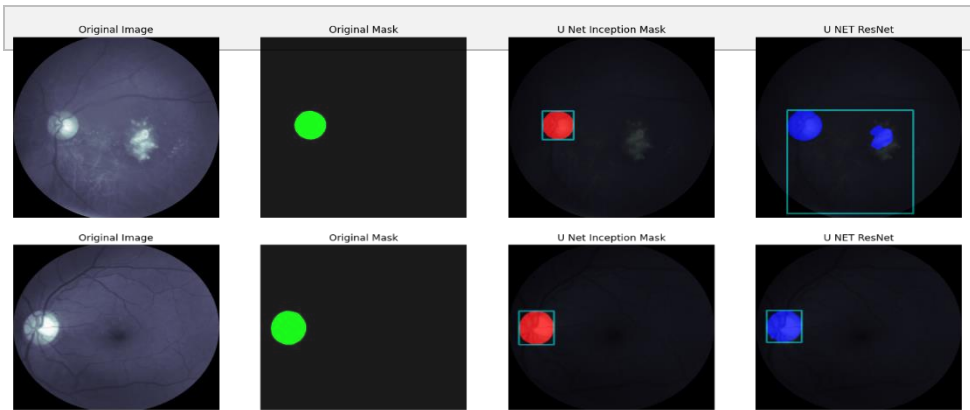
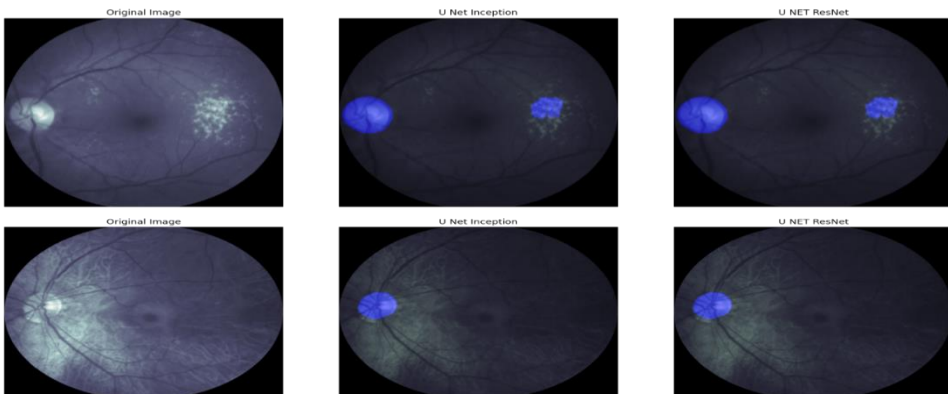


Fig. 7. Mask prediction and BBox using Dense-ED-UHI: Encoder-Decoder based Unet Hybrid Inception ( Proposed Model ).

The results of the AMD recognition models and statistical analysis using the Dense-ED-UHI based on Table 4, respectively, show that the Encoder Decoder-based Unet Hybrid Inception architecture is shown in the following Table. Table 4 presents statistics, including mean, standard deviation, minimum, maximum, and quartiles for various performance metrics across the dataset. Metrics such as loss, accuracy, binary accuracy, the area under the curve (AUC), specificity, and sensitivity are analyzed, indicating overall high performance with minor variations observed.

Considering the median values, the algorithm's median loss is 0.776345, indicating that it minimizes prediction errors throughout the learning process. The framework's mean accuracy and binary accuracy, both of which are 0.994058, demonstrate its excellent general accuracy in forecasting and accurate identification of the positive category in binary categorization tasks. With an average AUC of 0.991351, the model is very capable of distinguishing between positive and negative data. The system's ability to identify the negative category is measured by its average particularity, which is 0.994315, while its ability to recognize the positive category is measured by its mean sensitivity, which is 0.979943.



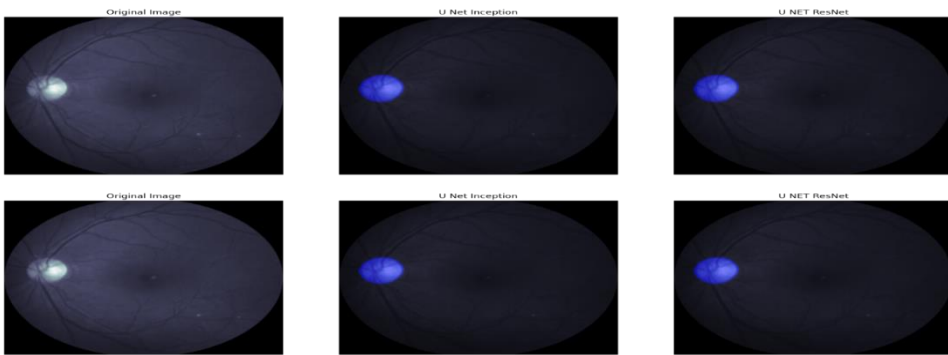


Fig. 8. Comparison with other state of the art backbone ( Resent50).

Table 4. Summary of Metrics Distribution.

Metric	loss	accuracy	binary accuracy	auc	Specificity	Sensitivity
mean	0.776345	0.994058	0.994058	0.991351	0.994315	0.987943
std	0.007104	0.001522	0.001522	0.010562	0.001358	0.018523
min	0.759107	0.990069	0.990069	0.964889	0.990533	0.931444
25 %	0.771469	0.992902	0.992902	0.989458	0.993515	0.968609
50 %	0.776116	0.994475	0.994475	0.997225	0.994529	0.987165
75 %	0.780667	0.995228	0.995228	0.998594	0.995411	0.993777
max	0.796842	0.996465	0.996465	0.999433	0.996659	0.999816

Analyzing the average standard deviations (std), figures allows us to see that there is not much variety in the measurements. This demonstrates that the algorithm's effectiveness remains consistent across different test sets or data sets. The lowest values represent the lowest performances discovered and the bottom bounds of the measurements. The percentages at the 25th percentile reflect the accuracy of the model at lower levels; the numbers at the 50th percentile (median) represent the halfway point, and the figures at the 75th percentile show the broader range. The highest values represent the utmost limits of the metrics and the highest efficiency that was discovered.

The aforementioned figure's statistics column and box plots provide an overview of the framework's performance across a number of measures. The standard numbers represent the range of the model, while its mean principles indicate its overall average efficiency. Examining the lowest, mean, 75th percentile, and maximum values reveals the model's effectiveness over a variety of values. Overall, the algorithm performs well, with excellent marks for sensitivity, area under the curve particularity, dichotomous accuracy, and precision. The framework's consistent accuracy and low volatility suggest that it is reliable and capable of producing accurate projections.

## 5. Conclusion

While aging is the primary cause of AMD and diabetes is the primary cause of diabetic retinopathy, both conditions are complex, multifactorial illnesses, and our knowledge of

both is always evolving. Our techniques for classifying them have changed a lot over the years, and we've had to adjust them to stay up with advancements in technology and medicine. The huge advances in artificial intelligence, artificial intelligence-driven disease pathophysiology, imaging technology, and therapy that have occurred over the previous several decades must be considered in any new categorization system. The model's accuracy in both the training and test sets was 92.5 %, indicating its ability to draw valid conclusions about data that has not been seen. The model's utility is further shown by recall scores of 99.1 % for AMD and 92.9 % for non-AMD. The system demonstrates its ability to accurately identify AMD in retinal images, with accuracy levels of over 99.9 % across training, testing, and validation datasets. When it comes to AMD, the mathematical models are very exact and precise, with a median accuracy of 99.4 %. Their 99.7 % AUC scores show the models' ability to discriminate between favorable and unfavorable instances. Their 98.7 % sensitivity scores show the models' ability to identify true positives. With a high specificity of 99.4 %, the models are able to classify negative cases with accuracy. In conclusion, the newly developed AMD classification algorithms, incorporating pixel-wise periodic shuffling convolution alongside customized U-Net models like Dense-ED-UHI, demonstrate promising advancements in retinal disease segmentation. These models exhibit superior performance, particularly in terms of accuracy and specificity, surpassing other assessed methods. Their ability to accurately detect and differentiate between retinal illnesses signifies their reliability and efficiency. A key advantage of the Dense-ED-UHI architecture lies in its ability to gather both local and global contextual information, utilizing multi-scale properties to capture precise details in retinal images. Further exploration of the RDCNN model's potential for categorization in databases is warranted, given its promising results in photo segmentation tasks. In summary, leveraging deep learning models, including UHI and potentially RDCNN, holds significant promise for improving the segmentation of retinal diseases. These models demonstrate exceptional accuracy, robustness, and potential for early detection and diagnosis, contributing to advancements in healthcare through continued research and development in this area.

## References

1. <https://www.visionmonday.com/business/research-and-stats/article/us-blindness-rates-are-expected-to-double-by-2050-cdc-says> (Accessed on January 13, 2023).
2. H. Wang, K. K. Lung Chong, and Z. Li, Applications of AI to Age-Related Macular Degeneration: a Case Study and a Brief Review - 2022 *Int. Conf. on Computer Engineering and Artificial Intelligence (ICCEAI)* (Shijiazhuang, China, 2022) pp. 586-589. <https://doi.org/10.1109/ICCEAI55464.2022.00125>
3. A. Bali and V. Mansotra, Deep Learning-based Techniques for the Automatic Classification of Fundus Images: A Comparative Study - 3rd *Int. Conf. on Advances in Computing, Communication Control and Networking (ICAC3N)* (Greater Noida, India, 2021) pp. 351-359. <https://doi.org/10.1109/ICAC3N53548.2021.9725464>
4. A. Bali and V. Mansotra, *Arch Comput. Methods Eng.* **31**, 487 (2023). <https://doi.org/10.1007/s11831-023-09989-8>
5. A. Bali and V. Mansotra, *FUNDUS and OCT Image Classification Using DL Techniques*, in *Rising Threats in Expert Applications and Solutions*, ed. V. S. Rathore et al. (Springer, Singapore, 2022). [https://doi.org/10.1007/978-981-19-1122-4\\_8](https://doi.org/10.1007/978-981-19-1122-4_8)



6. S. Muchuchuti and S. Viriri, J. Imaging **9**, 84 (2023). <https://doi.org/10.3390/jimaging9040084>
7. M. Wu, Y. Lu, X. Hong, J. Zhang, B. Zheng et al., Front. Comput. Neurosci. **16**, ID 1079155 (2022). <https://doi.org/10.3389/fncom.2022.1079155>
8. A. Bali and V. Mansotra, An Overview of Retinal Image Classification-Techniques and Challenges - *First Int. Conf. on Advances in Computing and Future Communication Technologies* (ICACFCT) (Meerut, India, 2021), pp. 91-97. <https://doi.org/10.1109/ICACFCT53978.2021.9837371>
9. J. H. Tan, S. V. Bhandary, S. Sivaprasad, Y. Hagiwara, A. Bagchi et al., Future Generation Comput. Systems **87**, 127 (2018). <https://doi.org/10.3390/diagnostics10050261>
10. J. Y. Choi, T. K. Yoo, J. G. Seo, J. Kwak, T. T. Um and T. H. Rim, PLoS One **12**, ID e0187336 (2017). <https://doi.org/10.1371/journal.pone.0187336>
11. T. K. Yoo, J. Y. Choi, J. G. Seo, B. Ramasubramanian, S. Selvaperumal et al., Med. Biol. Eng. Comput. **57**, 677 (2019). <https://doi.org/10.1007/s11517-018-1915-z>
12. A. Govindaiah, M. A. Hussain, R. T. Smith, and A. Bhuiyan et al., Deep Convolutional Neural Network Based Screening and Assessment of Age-Related Macular Degeneration from Fundus Images - *Proc. IEEE 15th Int. Symp. on Biomedical Imaging (ISBI)* (Washington, DC, USA, Apr. 2018) pp. 1525–1528. <https://doi.org/10.1109/ISBI.2018.8363863>
13. C. Pereira, L. Gonçalves, and M. Ferreira, Informat. Sci. **296**, 14 (2015). <https://doi.org/10.1016/j.ins.2014.10.059>
14. A. Ganjdanesh, J. Zhang, E. Y. Chew, Y. Ding, H. Huang, and W. Chen, PNAS Nexus **1**, pgab003 (2022). <https://doi.org/10.1093/pnasnexus/pgab003>
15. S. Kadry, V. Rajinikanth, R. G. Crespo, and E. Verdú, J. Supercomput. **78**, 7321 (2022). <https://doi.org/10.1007/s11227-021-04181-w>
16. A. Bali and V. Mansotra, Int. J. Adv. Comput. Sci. Appl. **12**, 537 (2021). <https://doi.org/10.14569/IJACSA.2021.0121269>
17. A. Bali and V. Mansotra, Multimedia Tools Appl. **83**, 49813 (2023). <https://doi.org/10.1007/s11042-023-17530-z>
18. R. O. Ogundokun, A. T. Abdulahi, A. R. Adenike, A. N. Babatunde, and R. S. Babatunde, Inception V3 Based Approach for the Recognition of Age-related Macular Degeneration Disease - *Int. Conf. on Science, Engineering and Business for Sustainable Development Goals (SEB-SDG)* (Omu-Aran, Nigeria, 2023), pp. 1-7. <https://doi.org/10.1109/SEB-SDG57117.2023.10124539>
19. F. Ajesh and A. Abraham, Age-Related Macular Degeneration using Deep Neural Network Technique and PSO: A Methodology Approach, in *Intelligent Systems Design and Applications*, ed. A. Abraham et al. (Springer, Cham, 2023). [https://doi.org/10.1007/978-3-031-35501-1\\_6](https://doi.org/10.1007/978-3-031-35501-1_6)
20. J. Morano, Á. S. Hervella, J. Rouco, J. Novo, J. I. Fernández-Vigo et al., Comput. Methods Programs Biomed. **229**, ID 107296 (2023). <https://doi.org/10.1016/j.cmpb.2022.107296>
21. J. Niu, S. Dong, Q. Yu, K. Dang, and X. Ding - *IEEE 20th Int. Symp. on Biomedical Imaging (ISBI)* (Cartagena, Colombia, 2023), pp. 1-52023. <https://doi.org/10.1109/ISBI53787.2023.10230619>
22. S. Tang, Z. Qi, J. Granley, and M. Beyeler, U-Net with Hierarchical Bottleneck Attention for Landmark Detection in Fundus Images of the Degenerated Retina, in *Ophthalmic Medical Image Analysis*, ed. H. Fu et al. (Springer, Cham, 2021). [https://doi.org/10.1007/978-3-030-87000-3\\_7](https://doi.org/10.1007/978-3-030-87000-3_7)
23. H. Fu, F. Li, J. I. Orlando, H. Bogunovic, X. Sun et al., IEEE Dataport (2020). <https://dx.doi.org/10.21227/dt4f-rt59>
24. X. Leng, R. Shi, Y. Wu, S. Zhu, X. Cai et al., PLoS ONE **18**, ID e0284060 (2023). <https://doi.org/10.1371/journal.pone.0284060>